



HAL
open science

In situ Laser Induced Breakdown Spectroscopy as a tool to discriminate volcanic rocks and magmatic series, Iceland.

Clément P.M. Roux, J. Rakovský, Olivier Musset, Fabrice Monna, Jean-François Buoncristiani, Pierre Pellenard, Christophe Thomazo

► To cite this version:

Clément P.M. Roux, J. Rakovský, Olivier Musset, Fabrice Monna, Jean-François Buoncristiani, et al.. In situ Laser Induced Breakdown Spectroscopy as a tool to discriminate volcanic rocks and magmatic series, Iceland.. Spectrochimica Acta Part B: Atomic Spectroscopy, 2015, 103-104, pp.63-69. 10.1016/j.sab.2014.11.013 . hal-01096389

HAL Id: hal-01096389

<https://hal.science/hal-01096389v1>

Submitted on 21 Mar 2023

HAL is a multi-disciplinary open access archive for the deposit and dissemination of scientific research documents, whether they are published or not. The documents may come from teaching and research institutions in France or abroad, or from public or private research centers.

L'archive ouverte pluridisciplinaire **HAL**, est destinée au dépôt et à la diffusion de documents scientifiques de niveau recherche, publiés ou non, émanant des établissements d'enseignement et de recherche français ou étrangers, des laboratoires publics ou privés.



Distributed under a Creative Commons Attribution 4.0 International License

In situ Laser Induced Breakdown Spectroscopy as a tool to discriminate volcanic rocks and magmatic series, Iceland

C.P.M. Roux ^{a,*}, J. Růžek ^a, O. M. Ússe ^t, F. Mon ^m, J.-F. Buoncristiani ^c, P. P. d'Énard ^c, C. Thomazo ^c

^a Laboratoire interdisciplinaire Carnot de Bourgogne, UMR 6303 CNRS-Université de Bourgogne, BP 47 870, F-21078 Dijon Cedex, France

^b Laboratoire ARTéHIS, UMR 6298 CNRS-Université de Bourgogne, 6 Boulevard Gabriel, F-21000 Dijon, France

^c Laboratoire Biogéosciences, UMR 6282 CNRS-Université de Bourgogne, 6 Boulevard Gabriel, F-21000 Dijon, France

This study evaluates the potentialities of a lab-made pLIBS (portable Laser-Induced Breakdown Spectroscopy) to sort volcanic rocks belonging to various magmatic series. An in-situ chemical analysis of 19 atomic lines, including Al, Ba, Ca, Cr, Cu, Fe, Mg, Mn, Na, Si, Sr and Ti, from 21 sampled rocks was performed during a field exploration in Iceland. Iceland was chosen both for the various typologies of volcanic rocks and the rugged conditions in the field in order to test the sturdiness of the pLIBS. Elemental compositions were also measured using laboratory ICP-AES measurements on the same samples. Based on these latter results, which can be used to identify three different groups of volcanic rocks, a classification model was built in order to sort pLIBS data and to categorize unknown samples. Using a reliable statistical scheme applied to LIBS compositional data, the classification capability of the pLIBS system is clearly demonstrated (90–100% success rate). Although this prototype does not provide quantitative measurements, its use should be of particular interest for future geological field investigations.

1. Introduction

Laser Induced Breakdown Spectroscopy (i.e. LIBS) is a technique used to take elementary chemical measurements on natural and synthetic samples regardless of whether they are solid, liquid or gaseous. It is based on the analysis of the radiation spectra of a plasma produced during laser irradiance [1,2] that was developed in the 1960's for the spectrochemical analysis of areas [3]. It is a versatile technique now widely used, for example, to measure pigments in paintings [4] and to perform quality control analyses [5]. The goal of the first study with a geological interest using this technique was to spot the elemental constituents of aqueous solutions [6]. Over the past decade, LIBS has been successfully applied to characterize rocks and minerals using mostly heavy laboratory equipment ([7,8] and references therein). One of the most striking examples is the operation of the Chemcam LIBS system on the Curiosity rover for the Mars Science Laboratory mission [9,10]. Thanks to recent technical advances, it is now possible to miniaturize the two main parts of the LIBS device, namely the laser and spectrometer, in order to carry them from the lab to the field. The gain in terms of compactness and outdoor operability is however offset by a notable loss in spectral resolution, sensitivity, and laser efficiency, precluding the traditional mathematical treatment of the LIBS spectra [11].

A portable LIBS system (pLIBS), easy to operate in field conditions (it fits in a backpack or a light suitcase, Fig. 1) has been recently developed

at the ICB laboratory at the Université de Bourgogne [12,13]. Its efficiency has already been demonstrated for distinguishing lithological variations from shale to volcanic ashes in a sediment core [13]. Outdoor applications to volcanic rock studies can now be envisaged. Among these applications, the direct classification of volcanic rocks into magmatic series (information not accessible without chemical analysis) would be very useful for geologists. Iceland is a good candidate to further test the capabilities of the pLIBS to fulfill this objective. As a matter of fact, Iceland includes fresh and recent basalt to rhyolite lavas of Late Pleistocene to Holocene age from tholeiitic to alkaline magmatic series. It is also a unique site in the world where recent magmatic activity, including several volcanic processes (hotspot and oceanic spreading ridge) has occurred. Because of the rugged Icelandic field conditions, another secondary objective can be pursued: to try out the pLIBS during remote geological field work. The device obviously has to be resistant to the vibrations caused by transportation in a 4-wheel drive as well as to temperature variations.

In practice, a set of volcanic rocks was sampled and measured in the field using the pLIBS. Once back at the laboratory, a bulk powder analysis using classical laboratory ICP-AES was performed to sort the rocks in terms of the magmatic series. Provided that this information was known, a state-of-the-art supervised statistical learning process (see [14] and references cited therein), including the preparation of training data with a compositional approach followed by a discriminant analysis, was used to treat the pLIBS measurements. The pertinence of the obtained model was then evaluated by two methods: a leave-one-out cross-validation and the posterior attribution of control samples, for

* Corresponding author. Tel.: +33 3 80 39 59 41; fax: +33 3 80 39 59 71.
E-mail address: clement.roux@u-bourgogne.fr (C.P.M. Roux).



Fig. 1. Portable LIBS system and its two main parts, connected together by an umbilical. Photo from J.-F. Buoncristiani.

which the membership is known. As a result, the possibilities of the pLIBS system to classify volcanic rocks into magmatic series in the field are discussed.

2. Material and methods

2.1. Geological setting and sampling

Iceland is located on the North Mid-Atlantic Ridge plate boundary, which separates the Eurasian and North American plates. It results from the volcanism formed by the coincidence of the spreading boundary of these plates and by a hotspot called the “Iceland plume” [15,16]. Iceland’s magmatic rocks, related to different geodynamical contexts, range from mafic (i.e. basalts) to silicic lavas (i.e. rhyolites). Three volcanic series, categorized by their chemical and mineralogical characteristics, are defined: tholeiitic, sub-alkaline and transitional alkaline series

[17,18]. Based on the examination of the geological map and petrographic observations in the field, a total of 21 sites (Fig. 2), located in the south-western part of the island, were selected. The goal was to sample a collection of rocks representing, as much as possible, the different kinds of volcanic rocks and magmatic series outcropping within this area. At each location, two rock samples (hereafter called A and B), freshly cut in the field, were collected (ca. 200 g each). The texture of these selected rocks ranges from microlithic to vitreous. They were measured using the LIBS portable device before storage for later ICP-AES analysis.

2.2. LIBS technique

2.2.1. The portable LIBS system

The gun-shaped prototype developed at the ICB Laboratory incorporates a pulsed Nd^{3+} :YAG flash lamp laser, that emits in infrared at a

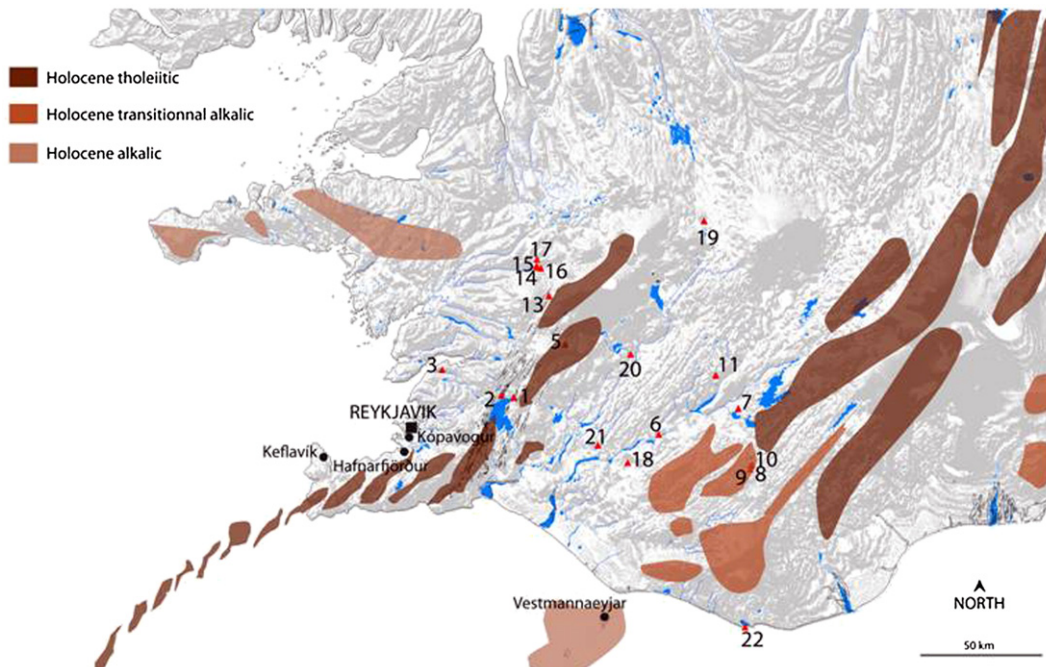


Fig. 2. Map of Iceland with volcanic zones [23] and sampling sites.

wavelength of 1064 nm. Although the device has a double pulse capability [19,20], no advantage was recognized in applying this type of regime to volcanic rocks, and therefore, the laser was always operated in single pulse mode (maximum 1 Hz). The duration of a pulse is approximately 5 ns and the energy delivered reaches 40 mJ. The output laser beam is magnified by a $\times 2$ telescope to divide the laser spot diameter by two at the focal point of a 50 mm lens. The irradiance is above the ablation threshold of most materials (about 1 GW/cm²) using a spot diameter of 400 μ m. The depth of focus, defined as $2 \times$ the Rayleigh length, is approximately 7 mm. A transparent silica window located between the sample and focusing lens protects the laser from particles generated by ablation. This is done inside a hollow aluminum cone, corresponding to the analysis chamber. A membrane pump is used to evacuate the shot residues, which could damage the silica window. The whole configuration renders the device safe because laser shots are only possible when there is direct contact between the sample and aluminum cone. The precision of the shot location is ensured by two crossed red laser beams and by a color camera pointed at the zone to be analyzed. The plasma light generated by the laser shot is collected through the silica window with an aspheric lens and transmitted to the spectrometer by a transport fiber. A small casing containing the spectrometer, batteries, the pump and its filter, and the computer is connected to the gun by an umbilical. The spectrometer is a compact, wide range, triggered, Czerny-Turner Ocean Optics HR 2000+. Its bandwidth ranges from 200 nm to 650 nm in wavelength, with an optical resolution of ca. 0.4 nm, corresponding to a spectral resolution of approximately 1000. Its minimum integration time is 1 ms. The wavelength calibration of the spectrometer is corrected from temperature variations, which are recorded using an embedded probe. The intensity of the spectrometer is calibrated at the laboratory to take into account the low sensitivity of the CCD detector in the UV range, and the highly variable efficiency of the grating. The spectrum is analyzed by an embarked laptop via a lab-made software suite [13]. The system is completely autonomous, with an operating time limited to approximately 6 h, corresponding to the lifetime of the computer battery. Its total mass is ca. 5 kg, computer included (without the backpack or the suitcase), making it easy to carry in the field. It was transported in a standard plastic suitcase with foam stuffing. The suitcase was placed in the trunk of the vehicle without any particular precaution, and was therefore subject to shocks and vibrations.

2.2.2. In-field LIBS measurements

Given that volcanic rocks can be heterogeneous and that laser shots are by definition punctual, large variations in the measurements are

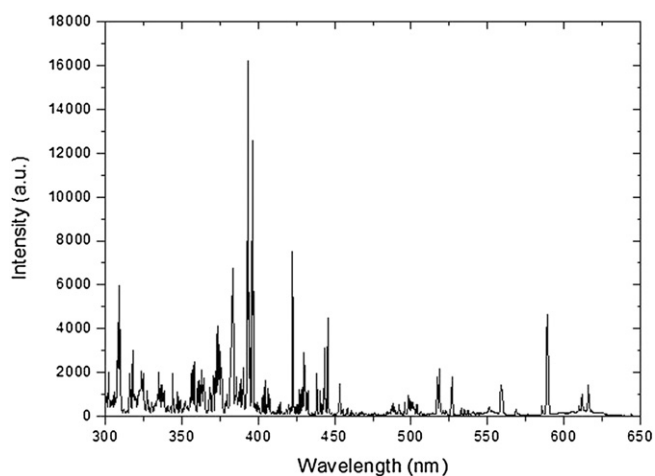


Fig. 3. Example of a raw spectrum (sample 21A) obtained in the field before normalization. The acquisition is performed between 300 nm and 650 nm. Note that the Y-axis is expressed with an arbitrary unit.

expected for the same sample. It is necessary to set up an experimental protocol to compensate for chemical heterogeneity. The experimental protocol, described below, was also designed to reduce the thermal and random noise of the detector. Measurements were organized into 15 spectra (Fig. 3), each of them consisting of an accumulation of 10 individual shots performed at 10 different locations, randomly chosen on the surface of the rock. This number of shots is limited in order to reduce the acquisition time of one single spectrum to 10 s, which is compatible with a hand-held system. The atomic species were identified by comparing the position of the observed lines to the atomic wavelengths listed in two reference databases [21,22]. The lines chosen must be much greater than the spectrometer noise, and each of them must be properly isolated from the others. A total of 19 atomic lines, useful to characterize volcanic rocks, were retained: Al, Ba, Ca, Cr, Cu, Fe, Mg, Mn, Na, Si, Sr and Ti. Their peak areas were calculated by integrating the signals between the two boundaries reported in Table 1. Raw data for the 19 lines are obtained by averaging the areas of the 15 spectra. Coefficients of variations are typically ca. 10–20% for each line. All of the samples belonging to both the A and B series were measured in the field as described above.

2.3. In-laboratory determination of the elemental compositions

Approximately 500 mg of finely powdered samples (<100 μ m) belonging to series A was measured for their major elements expressed as wt.%, and for Ba and Sr by Actlabs, Ontario, Canada (Table 2). Total digestion was achieved by lithium metaborate/tetraborate fusion, followed by nitric acid dissolution. The solutions were then measured by ICP-AES. A set of certified reference materials (CRMs): NIST 694, DNC-1, GBW 07113, W-2a, SY-4, BIR-1a, was measured in the same batch. The concentrations appear to be within ± 1 –5% of the certified values, when the concentrations are sufficiently above the detection limits. Sample 9A was duplicated, providing deviations between both measurements below $\pm 3\%$ for the major and trace elements.

2.4. Statistical treatments

Statistical treatment, including a compositional analysis, was performed using the free R software (R Development Core Team, 2008, <http://www.r-project.org/>) with the MASS, compositions, rgr, kLaR, and Hotelling packages.

Table 1

Measured elements and their position lines corresponding to the maximum of the intensity. Low and high values represent the lower and upper limits in which the area of the peak is integrated.

Elements	Position (nm)	Low value (nm)	High value (nm)
Al I-a	# 309.2	308.7	309.6
Al I-b	# 394.1	393.8	394.5
Ba II	# 455.4	454.9	455.7
Ca I-a	# 422.5	422.0	422.9
Ca I-b	# 445.3	444.5	446.1
Cr I	# 358.0	357.4	358.9
Cu I	# 327.2	326.8	327.7
Fe I-a	# 373.4	372.8	373.9
Fe I-b	# 404.4	403.9	404.8
Fe I-c	# 438.2	437.7	438.7
Fe I-d	# 495.7	495.4	496.1
Mg I-a	# 517.1	516.0	517.8
Mg I-b	# 518.3	517.8	518.8
Mn I	# 403.0	402.4	403.6
Na I	# 588.9	587.8	590.4
Si	# 390.5	389.2	390.8
Sr I	# 460.7	460.2	461.0
Ti I-a	# 453.3	452.9	453.8
Ti I-b	# 498.1	497.6	498.5

Table 2
Elemental compositions of the collected rocks and corresponding detection limits.

Analyte symbol	SiO ₂	Al ₂ O ₃	Fe ₂ O ₃	MnO	MgO	CaO	Na ₂ O	K ₂ O	TiO ₂	P ₂ O ₅	Ba	Sr
	%	%	%	%	%	%	%	%	%	%	µg g ⁻¹	µg g ⁻¹
Detection limit	0.01	0.01	0.01	0.001	0.01	0.01	0.01	0.01	0.001	0.01	2	2
Sample												
1A	47.05	15.35	13.44	0.185	8.57	12.39	1.97	0.2	1.172	0.13	31	156
2A	47.41	15.22	13.1	0.192	9.44	11.95	1.92	0.13	1.433	0.11	27	153
3A	72.1	13.23	5.78	0.041	0.3	1.61	4.15	2.83	0.383	0.06	465	96
4A	44.52	12.3	20.48	0.264	5.1	9.71	2.6	0.47	3.365	0.37	96	196
5A	46.26	15.78	12.17	0.188	7.72	12.26	1.86	0.16	1.319	0.13	31	151
6A	49.37	15.36	12.83	0.188	6.54	12.16	2.43	0.2	1.839	0.15	47	202
7A	45.68	13.01	16.39	0.211	5.48	10.98	2.65	0.55	3.462	0.38	134	393
8A	64.64	14.28	6.44	0.128	0.77	2.27	5.09	3.55	0.486	0.08	454	142
9A	71.99	10.63	3.81	0.056	0.19	1.35	1.34	3.3	0.378	0.05	480	136
11A	46.23	13.62	14.95	0.21	9.31	11.22	1.95	0.22	1.957	0.19	49	171
12A	48.74	17.28	14.2	0.201	4.55	11.07	2.71	0.33	2.09	0.21	81	224
13A	73.49	11.77	6.4	0.081	0.21	1.28	4.13	3.1	0.147	0.01	600	82
14A	46.59	14.83	14.68	0.207	9.1	11.53	1.99	0.16	1.678	0.13	42	163
15A	51.22	12.68	14.48	0.239	2.68	6.61	2.78	0.25	2.951	1.04	110	307
16A	77.08	12.72	3.08	0.025	0.09	0.47	3.54	3.61	0.261	0.03	726	84
17A	48.28	15.77	12.06	0.183	8.17	12.26	2.1	0.18	1.101	0.11	33	131
18A	48.4	14.83	13.5	0.209	6.66	12.35	2.29	0.22	1.673	0.13	57	177
19A	48.38	13.81	16.29	0.215	5.7	11.62	2.25	0.36	2.105	0.22	77	155
20A	47.17	14.01	14.79	0.215	7.25	10.64	2.22	0.28	1.86	0.19	76	182
21A	44.85	12.34	18.15	0.224	5.23	10.55	2.34	0.37	3.566	0.27	87	242
22A	45.03	12.82	17.21	0.217	5.15	10.43	2.74	0.64	4.084	0.48	149	419

3. Results and discussion

3.1. In-field operability of the pLIBS

The pLIBS device developed at the ICB laboratory was subjected to the rugged conditions of a geological campaign: 2000 km on outback gravel trails and variable temperature (ca. 0 °C to 30 °C). No problems were noticed for either the laser or embedded electronics. Only the aspheric collect lens came off and the collect/lighting unit

came loose. These problems were easily repaired in the field within half an hour. The lens was fixed with nail polish and the collection/lighting unit was easily put back into the right position by using a brass reference sample, the spectral and intensity response of which is perfectly known. The pLIBS prototype therefore properly met our expectations for in situ analyses during a field mission, except for some minor problems that have to be fixed in the next version: for instance the touch screen appeared to be difficult to read in sunlight.

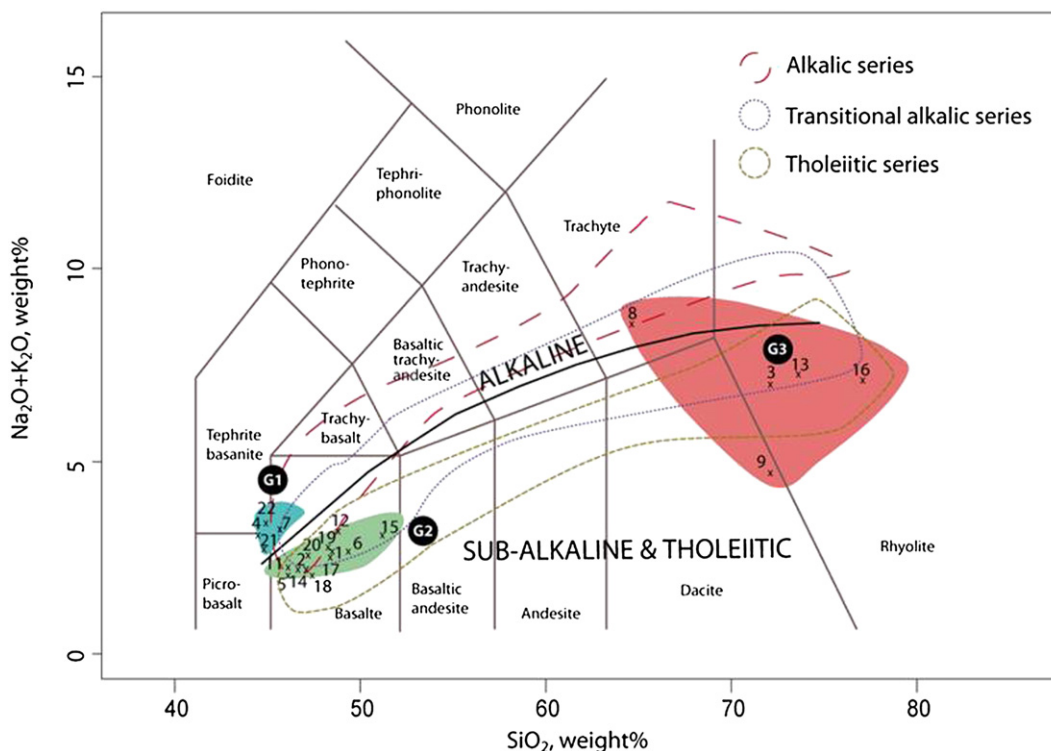


Fig. 4. Harker diagram representing Na₂O + K₂O versus SiO₂. The samples are positioned according to the ICP-AES results performed on series A. The envelopes of the magmatic series and the limit between the alkalic and sub-alkalic fields (dashed line) are from Jakobsson et al. [23] and Miyashiro [24], respectively.

Table 3

Pearson's coefficient correlations, r , between concentrations obtained after total digestion by ICP-AES and the normalized surface of the LIBS lines (see Table 2 for wavelength correspondence).

ICP-AES	LIBS	r	p -value
Al ₂ O ₃	Al I-a	0.368	0.100
	Al I-b	0.172	0.457
Ba	Ba II	0.776	<10 ⁻⁴ ***
	Ca I-a	0.828	<10 ⁻⁵ ***
CaO	Ca I-b	0.699	<10 ⁻³ ***
	Fe I-a	0.479	0.028*
Fe ₂ O ₃	Fe I-b	-0.470	0.031*
	Fe I-c	0.118	0.611
	Fe I-d	0.465	0.033*
	Mg I-a	0.528	0.013*
MgO	Mg I-b	0.675	<10 ⁻³ ***
	Mn I	0.483	0.027*
MnO	Na I	0.412	0.063
Na ₂ O	Si I	0.637	0.002**
SiO ₂	Sr I	0.580	0.005**
Sr	Ti I-a	0.236	0.302
TiO ₂	Ti I-b	0.217	0.345

* For $p < 0.05$.

** For $p < 0.01$.

*** For $p < 0.001$.

3.2. ICP-AES based chemical composition of volcanic rocks and classification

The usual way to discriminate between different volcanic rocks and magmatic series is to project the (Na₂O + K₂O) vs. SiO₂ chemical compositions in wt.% of samples in a Harker diagram where the nature of the volcanic rocks (e.g. basalt, rhyolite), defined by a range of chemical compositions and the boundaries between the magmatic series, are reported (Fig. 4). Most of the samples fall mainly within the basalt area while some rocks plot within the acidic domain (rhyolite, dacite, and trachyte). According to the database compiled by Jakobsson et al. [23], three groups corresponding to different magmatic rock series are defined (Fig. 4): (i) mafic alkalic series (G1, $n = 4$ samples), (ii) mafic tholeiitic-transitional alkalic series (G2, $n = 12$ samples), (iii) silicic tholeiitic-transitional alkalic series (G3, $n = 5$ samples).

3.3. Comparison of the LIBS and ICP-AES measurements

It has been attempted to correlate the concentrations measured by ICP-AES from homogeneous powders and the peak areas acquired from the pLIBS (Table 3). Several elements exhibit a significant positive linear relationship: Ba, Ca, Mg, Si, and Sr have a p -value < 0.01 and to a lesser extent, Mn and some of the Fe lines (p -value < 0.05), whereas other elements, such as Al, Na and Ti, are not correlated (p -value > 0.05). At best, the pLIBS system can be considered as a semi-quantitative technique because several factors, such as matrix effect, laser ablation efficiency, fluctuation in the plasma temperature, auto-absorption, etc., can notably blur the signal and make it difficult to interpret [25,26]. In the Harker diagram, it is necessary to use the sum of Na₂O + K₂O as the Y-axis, but the pLIBS-deduced Na peak area is not proportional to the true Na concentration while K is simply not assessed. Moreover, absolute concentrations are required. Even if the pLIBS-deduced Si peak areas are proportional to the SiO₂ contents, the calibration would need to be done beforehand in order to assess the true SiO₂ concentration using the pLIBS. This calibration would only be valid for one type of material. It is clear that it is not possible to straightforwardly assign the position of a rock in the volcanic series from the Harker diagram using the raw pLIBS dataset. Other solutions have therefore been developed.

3.4. Exploratory data analysis

It is a common procedure to divide the individual peak areas by the area of the whole spectrum thereby allowing the samples to be

compared between them [27,28]. Therefore, the 19 lines taken into account constitute a subset of the initial spectrum. They define a vector of D positive components (here $D = 19$), $\mathbf{x} = [x_1, \dots, x_D]$ summing up to a constant κ , with $\kappa \leq 1$. In this type of situation, it is common when working with the corresponding sub-composition to reclose the vector \mathbf{x} to 1 (e.g. [29]):

$$C(\mathbf{x}) = \left[\frac{x_1}{\sum_{i=1}^D x_i}, \dots, \frac{x_D}{\sum_{i=1}^D x_i} \right]$$

The closure operation transforms a positive vector of D positive components into a new vector $C(\mathbf{x})$ which maintains all of the ratios between the components. The subset of points after the closure of the D -dimensional real space is called simplex [30,31]. The compositional information is now only conveyed by the ratios between the components. At this point, it would be interesting to graphically visualize the structure of the multi-dimensional dataset in the aim of possibly identifying groups. Unfortunately, both the fully compositional data ($\kappa = 1$) and sub-compositional data ($\kappa < 1$) cannot be straightforwardly treated in terms of a principal component analysis, because the closure may lead to unstable or erroneous results with regard to the correlations [14]. A mathematical approach consists of first applying a centered log-ratio transformation, $clr(\cdot)$, to the compositions thereby avoiding the problems of spurious correlation and negative bias as described by Chayes [32]. The centered log-ratio transformation is defined by Aitchinson [30]:

$$clr(\mathbf{x}) = \left[\ln \frac{x_1}{g(\mathbf{x})}, \ln \frac{x_2}{g(\mathbf{x})}, \dots, \ln \frac{x_D}{g(\mathbf{x})} \right],$$

where $g(\mathbf{x})$ denotes the geometric mean of the parts: $g(\mathbf{x}) = (x_1, \dots, x_D)^{1/D}$. Then, the classical biplots can be made from this new set of coordinates (see [33] for further detail and how to read and interpret a bi-plot graph; [34]). For our purposes, the interesting feature of this modified version of the biplot is that it is equivalent to the analysis of all of the pairwise log-ratios [35]. As a consequence, the data are no longer treated

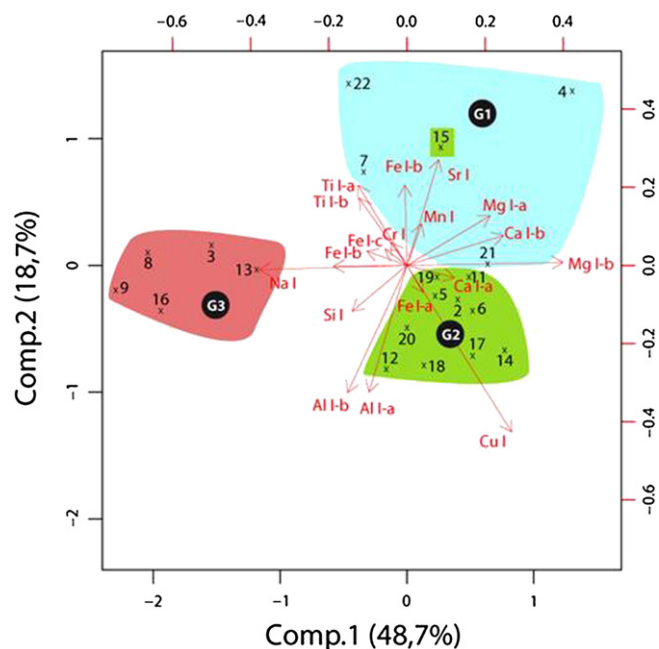


Fig. 5. Biplot using the 19 lines analyzed in the samples belonging to series A. The two first axes represent 48.7% and 18.7% of variance, respectively (i.e. a total close to 70%).

Table 4

Confusion matrix for the training data (i.e. 21 rock samples from series A). The prior probabilities are 1/3, 1/3, and 1/3 for each of the 3 groups.

		Actual group		
		G1	G2	G3
Predicted group	G1	4	0	0
	G2	0	12	0
	G3	0	0	5

in terms of absolute concentrations (information that cannot be accessed from pLIBS), but in terms of the spectrum morphology; i.e. by examining all of the possible pairwise log-ratios for the selected peaks.

The pLIBS measurement for the volcanic rocks is plotted using a biplot method because this representation preserves the distances between the individuals (Fig. 5). In our case, the percentages of variance explained by the two first axes are 48.7% and 18.7%, respectively; in other words, a total close to 70%. Based on the projection of the samples on the two first axes, the three groups previously identified by ICP-AES-based chemical analysis can be easily distinguished, except for sample 15A, which is visually moderately altered (Fig. 5). It is noteworthy that the second axis mainly separates G1 and G2, while the first axis secludes G3 from an ensemble constituted by G1 and G2. Even if these observations tend to indicate that the three groups of rocks can somehow be distinguished by the pLIBS analyses, they need to be explored further. It is better to use a multivariate analysis of variance (MANOVA) here in order to confirm the distinctiveness of the groups [36]. In addition, a discriminant analysis is needed to determine the rules for ascribing new (unknown) samples to these groups.

3.5. MANOVA and classification

It is not possible to directly perform a MANOVA on the previously clr-transformed data because the $clr(\cdot)$ is not injective, and therefore the covariance matrix is always singular. As an alternative, Egozcue et al. [37] developed a method called the ilr-transform (ilr for isometric log-ratio), which can be used to isometrically transform a composition in the D-part Aitchison-simplex into a (D-1) dimensional Euclidian vector. The ilr transformation is performed by following:

$$ilr(x) = z = [z_1, \dots, z_{D-1}]; z_i = \sqrt{\frac{i}{i+1}} \ln \sqrt{\frac{\prod_{j=1}^i x_j}{x_{i+1}}}, \text{ for } i = 1, \dots, D-1.$$

The covariance matrix of the ilr-transformed dataset is not singular. As a result, the multivariate analysis of variance can be directly calculated from the ilr coordinates in order to compare the multivariate population means of the three groups [38]. In this test, the null hypothesis is that the vector means are the same for all of the groups. This hypothesis must be rejected ($p < 10^{-9}$), meaning that at least one group is different from at least one other group. In addition, the three possible comparisons were performed as post hoc tests, using pairwise Hotelling's T^2

Table 5

Confusion matrix for the control data (i.e. 21 rock samples from series B considered as belonging to the same groups compared to their analogs belonging to series A). Calculations are made using the average spectrum of each sample. The prior probabilities are 1/3, 1/3, and 1/3 for each of the three groups.

		Actual group		
		G1	G2	G3
Predicted group	G1	3	0	0
	G2	1	12	0
	G3	0	0	5

Table 6

Confusion matrix for the control data (i.e. 21 rock samples from series B considered as belonging to the same groups compared to their analogs belonging to series A). Calculations are made using individual spectrum of each sample. The prior probabilities are 1/3, 1/3, and 1/3 for each of the three groups.

		Actual group		
		G1	G2	G3
Predicted group	G1	49	6	4
	G2	11	173	0
	G3	0	1	71

statistic [39]. Each group appears to be significantly different from the others (p is always < 0.007), even after a Bonferroni correction [40] which produces a familywise error rate α of 0.166 (0.05/3).

For the classification procedure, all of the pLIBS data obtained on the samples for which the membership to one of the three groups is known (i.e. the 21 samples belonging to series A, measured by ICP-AES) were first used as training data. The discriminant model was established after a stepwise forward variable/model selection using Wilks' Lambda criterion [41]. Four out of the eighteen variables appear to be significantly involved in the discrimination procedure ($p < 0.05$). With the leave-one-out cross-validation procedure, all of the samples are perfectly classified (Table 4). It is nonetheless difficult to identify the role of the original variables in the discrimination process because, although a back-transformation is always possible, the link between the ilr-transformed variables and the original data is lost in the transformation. As a consequence, it becomes quite complex to interpret the discriminant variables in terms of compositional parts. This should not represent a major drawback here, as we are more interested in the structure of the individuals with respect to their membership in the groups rather than in their composition. However elementary chemical concentrations are not provided here. In order to confirm the validity of the discriminant model built above, the 21 rocks belonging to series B (and sampled close to their analogs in series A) are now used as a control dataset. A total of 20 out of 21 samples are correctly recognized (Table 5), representing an excellent classification ability.

It could be also interesting to examine what the results would have been if the individual spectrum recorded for each sample had been used instead of their average. The 315 spectra (21 samples x 15 spectra) for series B were processed with the discriminant model built above. A total of 293 spectra out of 315 are now properly classified (Table 6). This suggests that once the learning process is done, the amount of time needed to perform the complete procedure can be divided by a factor 15, while still maintaining a high success rate. It should be noticed that this finding applies here because studied rocks do not contain large phenocrystals. If the studied samples had been more heterogeneous, i.e. with a grain size much bigger than beam size, the number of shot locations of at least 100 is desirable, as previously suggested [42].

4. Conclusion

A total of 21 volcanic rocks were analyzed by pLIBS in the field in Iceland, and later in laboratory by ICP-AES for the quantitative elemental compositions. These latter analyses sort the samples into three groups, used to train a discriminant model. Once the learning process has been achieved, the pLIBS system appears to be a powerful tool, and is able to classify rocks for which the chemical compositions are unknown. It might save considerable time saved in the field for the selection of samples. However, future studies including a greater diversity of magmatic rocks are needed for a comprehensive evaluation of the classification abilities of the LIBS system, in a more general context. In practice, the sturdiness of the pLIBS system has been demonstrated during a geological field trip.

Acknowledgments

We thank the Conseil Régional de Bourgogne for the support via the Synerjinov Program and the BQR (Bonus Qualité Recherche) for mission funding. We are grateful to the anonymous reviewer whose judicious comments have improved the manuscript.

References

- [1] D.A. Cremers, L.J. Radziemski, *Handbook of Laser-Induced Breakdown Spectroscopy*, Wiley and Sons, 2013.
- [2] D. Hahn, N. Omenetto, Laser-induced breakdown spectroscopy (LIBS), part II: review of instrumental and methodological approaches to material analysis and applications to different fields, *Appl. Spectrosc.* 166 (2012) 347–419, <http://dx.doi.org/10.1366/11-06574>.
- [3] Débras-Guédon, Liodec, De l'utilisation du faisceau d'un amplificateur à ondes lumineuses par émission induite par rayonnement (laser à rubis), comme source énergétique pour l'excitation des spectres d'émission des éléments, *C.R. Acad. Sci.* (1963) 3336–3339.
- [4] D. Anglos, S. Couris, C. Fotakis, Laser diagnostics of painted artworks: laser-induced breakdown spectroscopy in pigment identification, *Appl. Spectrosc.* 51 (1997) 1025–1030.
- [5] R. Noll, H. Bette, A. Brysch, M. Kraushaar, I. Mönch, L. Peter, V. Sturm, Laser-induced breakdown spectrometry applications for production control and quality assurance in the steel industry, *Spectrochim. Acta B* 56 (2001) 637–649, [http://dx.doi.org/10.1016/S0584-8547\(01\)00214-2](http://dx.doi.org/10.1016/S0584-8547(01)00214-2).
- [6] D.A. Cremers, L.J. Radziemski, T.R. Loree, Spectrochemical analysis of liquids using the laser spark, *Appl. Spectrosc.* 38 (1984) 721–729.
- [7] J. Cuiat, F. Fortes, L. Cabalin, F. Carrasco, M. Simón, J. Laserna, Man-portable laser-induced breakdown spectroscopy system for in situ characterization of karstic formations, *Appl. Spectrosc.* 62 (2008) 1250–1255.
- [8] R.S. Harmon, R.E. Russo, R.R. Hark, Applications of laser-induced breakdown spectroscopy for geochemical and environmental analysis: a comprehensive review, *Spectrochim. Acta B* 87 (2013) 11–26, <http://dx.doi.org/10.1016/j.sab.2013.05.017>.
- [9] S. Maurice, R. Wiens, M. Saccoccio, B. Barraclough, O. Gasnault, 6. m. authors, The ChemCam instrument suite on the mars science laboratory (MSL) rover: science objectives and mast unit description, *Space Sci. Rev.* 170 (2012) 95–166, <http://dx.doi.org/10.1007/s11214-012-9912-2>.
- [10] R. Wiens, S. Maurice, B. Barraclough, M. Saccoccio, W. Barkley, et al., The ChemCam instrument suite on the Mars Science Laboratory (MSL) Rover: body unit and combined system tests, *Space Sci. Rev.* 170 (2012) 167–227, <http://dx.doi.org/10.1007/s11214-012-9902-4>.
- [11] J.-B. Sirven, B. Bousquet, L. Canioni, L. Sarger, Laser-induced breakdown spectroscopy of composite samples: comparison of advanced chemometrics methods, *Anal. Chem.* 78 (2006) 1462–1469, <http://dx.doi.org/10.1021/ac051721p>.
- [12] J. Goujon, A. Giakoumaki, V. Piñon, O. Musset, D. Anglos, A. Georgiou, J. Boquillon, A compact and portable laser-induced breakdown spectroscopy instrument for single and double pulse applications, *Spectrochim. Acta B* 63 (2008) 1091–1096, <http://dx.doi.org/10.1016/j.sab.2008.08.019>.
- [13] J. Rakovsky, O. Musset, J. Buoncristiani, V. Bichet, F. Monna, P. Neige, P. Veis, Testing a portable laser-induced breakdown spectroscopy system on geological samples, *Spectrochim. Acta B* 74–75 (2012) 57–65, <http://dx.doi.org/10.1016/j.sab.2012.07.018>.
- [14] K. van den Boogaart, R. Tolosana-Delgado, *Analyzing Compositional Data With R*, Springer, 2013.
- [15] J.G. Schiilling, Iceland mantle plume: geochemical study of Reykjanes Ridge, *Nature* 242 (1973) 565–571, <http://dx.doi.org/10.1038/242565a0>.
- [16] T. Thordarson, G. Larsen, Volcanism in iceland in historical time: volcano types, eruption styles and eruptive history, *J. Geodyn.* 43 (2007) 118–152, <http://dx.doi.org/10.1016/j.jog.2006.09.005>.
- [17] E. Martin, O. Sigmarsson, Crustal thermal state and origin of silicic magma, *Contrib. Mineral. Petrol.* 153 (2007) 593–605, <http://dx.doi.org/10.1007/s00410-006-0165-5>.
- [18] O. Sigmarsson, S. Steinthorsson, Origin of Icelandic basalts: a review of their petrology and geochemistry, *J. Geodyn.* 43 (2007) 87–100, <http://dx.doi.org/10.1016/j.jog.2006.09.016>.
- [19] J. Uebbing, J. Brust, W. Sdorra, F. Leis, K. Niemax, Reheating of a laser-produced plasma by a second pulse laser, *Appl. Spectrosc.* 145 (1995) 1419–1423.
- [20] V. Badushok, F. DeLucia Jr., J. Gottfried, C. Munson, A. Miziolek, Double pulse laser ablation and plasma: laser induced breakdown spectroscopy signal enhancement, *Spectrochim. Acta B* 161 (2006) 999–1014.
- [21] R. Kurucz, B. Bell, *Atomic Line Data Kurucz*, 1995.
- [22] Y. Ralchenko, A. Kramida, J. Reader, NIST Atomic Spectra, Database 3.1.5, 2008.
- [23] S. Jakobsson, K. Jónasson, I. Sigurdsson, The three igneous rock series of Iceland, *JÖKULL* 58 (2008) 117–138.
- [24] A. Miyashiro, Nature of alkalic volcanic rock series, *Contrib. Mineral. Petrol.* 66 (1978) 91–104.
- [25] J.M. Anzano, M.A. Villoria, A. Ruiz-Medina, R.J. Lasheras, Laser-induced breakdown spectroscopy for quantitative spectrochemical analysis of geological materials: effects of the matrix and simultaneous determination, *Anal. Chim. Acta.* 575 (2006) 230–235, <http://dx.doi.org/10.1016/j.aca.2006.05.077>.
- [26] V. Lazić, R. Barbini, F. Colao, R. Fantoni, A. Palucci, Self-absorption model in quantitative laser induced breakdown spectroscopy measurements on soils and sediments, *Spectrochim. Acta B* 56 (2001) 807–820, [http://dx.doi.org/10.1016/S0584-8547\(01\)00211-7](http://dx.doi.org/10.1016/S0584-8547(01)00211-7).
- [27] D. Body, B. Chadwick, Optimization of the spectral data processing in a LIBS simultaneous elemental analysis system, *Spectrochim. Acta B* 56 (2001) 725–736, [http://dx.doi.org/10.1016/S0584-8547\(01\)00186-0](http://dx.doi.org/10.1016/S0584-8547(01)00186-0).
- [28] J. Tucker, M. Dyar, M. Schaefer, S. Clegg, R. Wiens, Optimization of laser-induced breakdown spectroscopy for rapid geochemical analysis, *Chem. Geol.* 277 (2010) 137–148, <http://dx.doi.org/10.1016/j.chemgeo.2010.07.016>.
- [29] J. Egozcue, Pawlowsky-Glahn, Groups of parts and their balances in compositional data analysis, *Math. Geol.* 37 (2005) 795–828, <http://dx.doi.org/10.1007/s11004-005-7381-9>.
- [30] J. Aitchison, *The Statistical Analysis of Compositional Data*, Chapman & Hall, London, 1986.
- [31] C. Barceló-Vidal, J. Martín-Fernández, V. Pawlowsky-Glahn, Mathematical foundations of compositionnal data analysis, *Proceedings of IAMG*, 2001.
- [32] F. Chayes, On correlation between variables of constant sum, *J. Geophys. Res.* 65 (1960) 4185–4193, <http://dx.doi.org/10.1029/JZ065i012p04185>.
- [33] J. Aitchison, M. Greenacre, Biplots of compositional data, *Appl. Stat.* 51 (2002) 375–392, <http://dx.doi.org/10.1111/1467-9876.00275>.
- [34] J. Daunis-i-Estadella, C. Barceló-Vidal, A. Buccianti, Exploratory compositional data analysis, *Geol. Soc. Lond., Spec. Publ.* 264 (2006) 161–174, <http://dx.doi.org/10.1144/GSL.SP.2006.264.01.12>.
- [35] J. Daunis-i-Estadella, S. Thió-Henestrosa, G. Mateu-Figueras, Including supplementary elements in a compositional biplot, *Comput. Geosci.* 37 (2011) 696–701, <http://dx.doi.org/10.1016/j.cageo.2010.11.003>.
- [36] D. Hand, C. Taylor, *Multivariate Analysis of Variance and Repeated Measures*, Chapman and Hall, 1987.
- [37] J. Egozcue, V. Pawlowsky-Glahn, G. Mateu-Figueras, C. Barceló-Vidal, Isometric log ratio transformations for compositional data analysis, *Math. Geol.* 35 (2003) 279–300 (0882-8121/03/0400-0279/1).
- [38] L. Kovacs, G. Kovacs, J. Martín-Fernández, C. Barceló-Vida, Major-oxyde compositionnal discrimination in Cenozoic volcanites of Hungary exploratory, *Geol. Soc. Lond., Spec. Publ.* 264 (2006) 11–23, <http://dx.doi.org/10.1144/GSL.SP.2006.264.01.02>.
- [39] H. Hotelling, The generalization of student's ratio, *Ann. Math. Stat.* 2 (1931) 360–378, <http://dx.doi.org/10.1214/aoms/1177732979>.
- [40] J. Bland, D. Altman, Multiple significance tests: the Bonferroni method, *BMJ* 310 (1995) 170.
- [41] K. Mardia, J. Kent, J. Bibby, *Multivariate Analysis*, Academic Press, 1979.
- [42] M.C. McCanta, P.A. Dobosh, M.D. Dyar, H.E. Newsom, Testing the veracity of LIBS analyses on Mars using the LIBSSIM program, *Planet. Space Sci.* 81 (2013) 48–54, <http://dx.doi.org/10.1016/j.pss.2013.03.004>.